

Hindlimb gait defects due to motor axon loss and reduced distal muscles in a transgenic mouse model of Charcot–Marie–Tooth type 2A

Scott A. Detmer¹, Christine Vande Velde², Don W. Cleveland² and David C. Chan^{1,*}

¹Division of Biology, California Institute of Technology, 1200 East California Boulevard, MC114-96, Pasadena, CA 91125, USA and ²Ludwig Institute, University of California, San Diego, 9500 Gilman Drive, La Jolla, CA 92093, USA

Received August 31, 2007; Revised October 15, 2007; Accepted October 22, 2007

Charcot–Marie–Tooth (CMT) disease type 2A is a progressive, neurodegenerative disorder affecting long peripheral motor and sensory nerves. The most common clinical sign is weakness in the lower legs and feet, associated with muscle atrophy and gait defects. The axonopathy in CMT2A is caused by mutations in *Mitofusin 2* (*Mfn2*), a mitochondrial GTPase necessary for the fusion of mitochondria. Most *Mfn2* disease alleles dominantly aggregate mitochondria upon expression in cultured fibroblasts and neurons. To determine whether this property is related to neuronal pathogenesis, we used the HB9 promoter to drive expression of a pathogenic allele, *Mfn2*^{T105M}, in the motor neurons of transgenic mice. Transgenic mice develop key clinical signs of CMT2A disease in a dosage-dependent manner. They have a severe gait defect due to an inability to dorsi-flex the hindpaws. Consequently, affected animals drag their hindpaws while walking and support themselves on the hind knuckles, rather than the soles. This distal muscle weakness is associated with reduced numbers of motor axons in the motor roots and severe reduction of the anterior calf muscles. Many motor neurons from affected animals show improper mitochondrial distribution, characterized by tight clusters of mitochondria within axons. This transgenic line recapitulates key motor features of CMT2A and provides a system to dissect the function of mitochondria in the axons of mammalian motor neurons.

INTRODUCTION

Charcot–Marie–Tooth disease (CMT) is a group of commonly inherited neuropathies characterized by loss of motor and sensory function in the longest peripheral nerves (1,2). Most CMT patients present clinically with lower leg weakness that is associated with loss of muscle mass and gait impairment. There are two main classifications of CMT based on the cell type affected. Demyelinating forms of CMT are the most common and are caused primarily by mutation of structural myelin proteins. In contrast, axonal forms of CMT directly disrupt the axons of peripheral nerves. CMT2A, an autosomal dominant disease, is the most common axonal CMT and is caused by mutations in *Mitofusin 2* (*Mfn2*) (3).

Mitofusins are mitochondrial outer membrane GTPases required for mitochondrial fusion from yeast to mammals

(4–6). Mammals have two mitofusins (*Mfn1* and *Mfn2*) that have partially redundant functions. Disruption of either *Mfn1* or *Mfn2* greatly reduces mitochondrial fusion, and loss of both abolishes all fusion. Over forty mutations in *Mfn2* have been identified from CMT2A patients (3,7–12). In the majority of cases, these mutations cause single amino acid substitutions within or adjacent to the GTPase domain.

Given its autosomal dominant inheritance pattern, CMT2A may be due to haploinsufficiency of *Mfn2* or dominant effects of the *Mfn2* mutants. These models are not mutually exclusive, and two observations support an involvement of the latter model. First, although many *Mfn2* disease alleles have loss-of-function mutations, others retain normal levels of mitochondrial fusion activity (13). Second, most *Mfn2* disease alleles dominantly cause mitochondrial aggregation when over-expressed in fibroblasts or cultured dorsal root ganglion

*To whom correspondence should be addressed. Tel: +1 6263952670; Fax: +1 6263958826; Email: dchan@caltech.edu

neurons (13,14). Such dominant activities would be expected to disrupt mitochondrial dynamics in peripheral neurons. In mammalian motor neurons, numerous mitochondria extend into the axon and densely pack into the terminal endings at the neuromuscular junction (15). Each terminal ending has been estimated to contain several hundred mitochondria (15). In *Drosophila*, mutants with defective recruitment of axonal mitochondria show aberrant synaptic transmission in photoreceptors (16) and motor neurons (17,18).

To determine whether *Mfn2* disease alleles have dominant effects *in vivo*, we generated transgenic mice expressing the pathogenic *Mfn2*^{T105M} allele in peripheral motor neurons. Mice homozygous for the transgene have defects very similar to motor defects found in CMT2A patients. They have a hindlimb gait impairment due to decreased hindlimb muscle mass and reduced number of motor axons. These phenotypes are associated with impaired distribution of axonal mitochondria in motor neurons. In addition to providing an animal model of CMT2A, this transgenic line may facilitate efforts to understand the role of axonal mitochondria in neuronal function.

RESULTS

Generation of *Mfn2*^{T105M} transgenic mouse

Given the dominant activity of *Mfn2* disease alleles in cultured cells (13,14), we reasoned that expression of such alleles in motor neurons of transgenic mice might lead to animal models that recapitulate CMT2A motor defects. For these studies, we chose the CMT2A allele *Mfn2*^{T105M}, which has been found in three unrelated CMT2A families to cause early-onset foot and leg muscular atrophy and additional features of scoliosis and ataxia (3,7,10). *Mfn2*^{T105M} localizes properly to mitochondria but is inactive for mitochondrial fusion (13) and induces mitochondrial aggregation when over-expressed (13,14). Residue T105 is in the middle of the GTPase G1 motif (103 GXXXXGKS 110) (19). To drive expression in motor neurons, we chose the homeobox HB9 promoter, whose selective expression in motor neurons has been documented in HB9-EGFP transgenic mice (20). Our transgene contains the HB9 promoter driving Myc-tagged *Mfn2*^{T105M} followed by an internal ribosomal entry sequence (IRES) and *EGFP* (Fig. 1A). Co-expression of the *IRES-EGFP* gene allows motor neurons and their processes to be readily identified.

Transgenic animals were identified by PCR analysis, and transgene expression was confirmed by western blot analysis with an anti-Myc antibody (Fig. 1B). One of the lines, termed *Tg1Mfn2*^{T105M} (hereafter referred to as simply *Mfn2*^{T105M}), is the subject of this study. To enable better characterization of this line and to rule out integration site effects, we used an inverse PCR strategy to clone the transgene integration site. Sequence analysis of the insertion site indicates that the transgene inserted into a non-coding region on chromosome 11 between genes *Rad51c* and *Ppm1e*. This integration site was confirmed by PCR reactions that flank the integration sites at both ends of the transgene (Fig. 1C). These genotyping assays also allowed us to readily distinguish

between heterozygous and homozygous *Mfn2*^{T105M} animals (Fig. 1C).

Transgene expression in motor neurons

As expected, the transgene is primarily expressed in the motor neurons. Transgenic embryos and newborn pups show EFGP-expressing neurons in the ventral portion of the developing spinal column (Fig. 2A and B). This staining pattern is identical to that found in control *HB9-EGFP* animals (data not shown). In transgenic animals, the EGFP-positive motor neurons also contain anti-Myc reactivity due to the tagged *Mfn2*^{T105M}-Myc transgene (Fig. 2A and B). Particularly in the embryonic day 12.5 samples, this anti-Myc staining is punctate within the cells, suggesting that the mitochondria are aggregated.

HB9 is expressed embryonically coincident with motor neuron formation (21,22), but its expression postnatally is less well documented. We monitored HB9 transgene expression in postnatal spinal cord samples by immunoblot. The *Mfn2*^{T105M} transgene is expressed with a time course similar to the control HB9-EGFP transgene (Fig. 2C). Both transgenes are expressed well during the first several days after birth but decline to very low levels by 3 weeks of age.

Hindlimb defect in homozygous *Mfn2*^{T105M} animals

Mfn2^{T105M} mice have several obvious defects depending on the dosage of the transgene. Heterozygous *Mfn2*^{T105M} mice are born with slightly shorter tails that have mild to moderate bony kinks or thickenings (Fig. 3A and B). In contrast, homozygous *Mfn2*^{T105M} animals have drastically shorter tails that are severely deformed (Fig. 3A, B and D–F).

Most remarkably, homozygous *Mfn2*^{T105M} animals have hindlimb and gait defects, evident from birth (Fig. 3D–F). These animals have limp hindpaws due to a failure to dorsi-flex at the ankle (Fig. 3D). When at rest, severely affected animals often fail to bring their hindpaws under their haunches and instead leave their hind limbs extended behind their bodies. Because of the defect in dorsi-flexion, homozygous mice have an abnormal gait characterized by dragging of the hindlimbs (Fig. 3E; Supplementary Material, Movie S1). In spite of this defect, the animals are active and walk with short pushes of the hindlimbs. In addition, the animals commonly have clenched hindpaws, due to an apparent inability to spread the toes (Fig. 3F). These phenotypes suggest that homozygous transgenic animals have severe weakness in the distal hindlimb muscles.

These hindlimb defects are incompletely penetrant and have variable expressivity. Of 85 homozygous transgenic animals, 60% were bilaterally affected, 26% were unilaterally affected and 14% were unaffected. No hindpaw defects were observed in heterozygous transgenic animals, even at 1 year of age. Homozygous animals have a 15% reduction in body weight at weaning (P20). The hindpaw defect does not appear to worsen with age, and no defect was observed in the forelimbs. Homozygous animals perform well on rota rod and beam walking assays (data not shown). Both heterozygous and homozygous animals are born at expected Mendelian ratios, live to greater than 1 year, and are fertile.

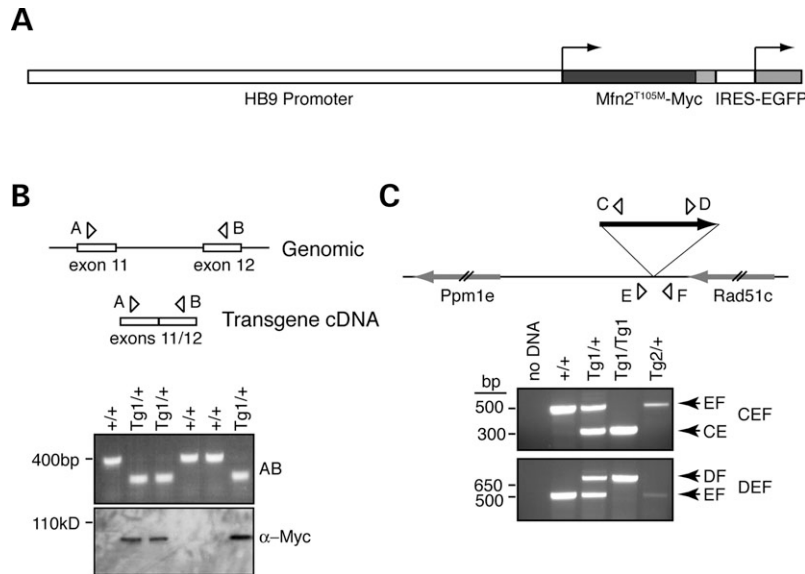


Figure 1. Generation of *Mfn2*^{T105M} transgenic mice. (A) Schematic of the transgenic construct. The motor-neuron-specific HB9 promoter drives expression of *Mfn2*^{T105M} (C-terminally tagged with Myc) and IRES-EGFP. (B) Identification of transgenic animals by PCR and western blotting. PCR amplification using primers A and B yield a 392 bp fragment from the genomic *Mfn2* locus and a 159 bp fragment from the *Mfn2* cDNA transgene, which lacks the intervening intron. The top gel shows PCR genotyping of embryonic day 12.5 embryos from a mating between a transgenic (*Mfn2*^{T105M/+}) and a wild-type animal. Note that in transgenic DNA samples, the smaller PCR product is favored over the longer endogenous product. The bottom panel is a western blot of spinal column lysates from the corresponding embryos, analyzed with an anti-Myc antibody. (C) In the *Mfn2*^{T105M} line, the transgene is integrated into chromosome 11 between the *Rad51c* and *Ppm1e* genes. The transgene is depicted as a single dark arrow, though there may be multiple tandem insertions. The top gel shows confirmation of the 5' integration site by PCR amplification using the C, E and F primers. The expected wild-type product (from primer pair EF) is 529 bp, and the transgene product (from primer pair EC) is 279 bp. The bottom gel shows confirmation of the 3' integration site by PCR with primers D, E and F. The transgene amplification product (from primer pair DF) is 800 bp. The genotypes of the samples are labeled above. *Tg2* is an independent *Mfn2*^{T105M} transgenic line.

Because only homozygous animals show hindlimb motor defects, we tested whether the transgene expression level corresponds with dosage. Western blot analysis indicated that homozygous animals at P0 and P8 contain approximately two-fold higher transgene expression than heterozygous animals (Fig. 3G). These results suggest that the hindlimb phenotype is dependent on transgene expression levels. Cloning of the transgene insertion site indicated that the transgene inserted into non-coding sequences (Fig. 1C), thereby arguing that the hindlimb phenotype is not caused by an insertion site effect.

The tail defects in homozygous *Mfn2*^{T105M} animals are also a consequence of transgene expression and not the integration site. In the course of these studies, we generated a second transgenic line (*Tg2Mfn2*^{T105M}) in which both heterozygotes and homozygotes have no phenotype. In this second transgenic line, the *Mfn2*^{T105M} transgene is expressed at only ~70% of *Tg1Mfn2*^{T105M} (Supplementary Material, Fig. S1A). However, compound heterozygotes between the two lines have tail defects that are intermediate in severity between *Mfn2*^{T105M/+} and *Mfn2*^{T105M/Mfn2} animals (Supplementary Material, Fig. S1B). These compound heterozygotes have no hindlimb phenotype. These observations suggest that the tail phenotype manifests at lower transgene expression levels than the hindlimb phenotype. We currently do not understand the pathogenesis of the tail phenotype, but interestingly, transgenic mice expressing the survival motor neuron gene 2 (SMN2) have loss of motor neurons and associated tail shortening (23).

Musculature defects in homozygous *Mfn2*^{T105M} animals

To understand the hindlimb defect in homozygous *Mfn2*^{T105M} animals, we analyzed the muscle mass in the lower hindlimb (Fig. 4A). At 22 days of age, compared to wild-type and *Mfn2*^{T105M/+} animals, *Mfn2*^{T105M/Mfn2} animals have dramatically reduced anterior musculature of the lower leg (Fig. 4B). In contrast, the posterior calf muscle mass is comparable across all genotypes. To quantify these observations, we dissected and weighed the anterior and posterior muscle of the distal hindlimb. We found that the masses of posterior calf muscles, normalized to animal body weight, are comparable between wild-type, *Mfn2*^{T105M} heterozygous and *Mfn2*^{T105M} homozygous animals (Fig. 4C). In contrast, the anterior muscles are dramatically smaller in homozygous *Mfn2*^{T105M} animals with affected hindlimbs (Fig. 4C). We found a similar reduction in anterior leg muscles at birth based on cryosections and at 8 months of age (data not shown). In homozygous *Mfn2*^{T105M} individuals with asymptomatic hindlimbs, the anterior muscles have an intermediate, variable mass (Fig. 4C).

This finding of reduced anterior muscles is consistent with the inability of affected homozygous animals to dorsi-flex at the ankle (Fig. 2D). Interestingly, weakness of the lower leg anterior peroneal muscle is a common symptom in CMT patients. CMT patients also have foot deformities, such as pes cavus and claw toes, due to weakness of foot muscles (1). We also found that the foot muscles in homozygous

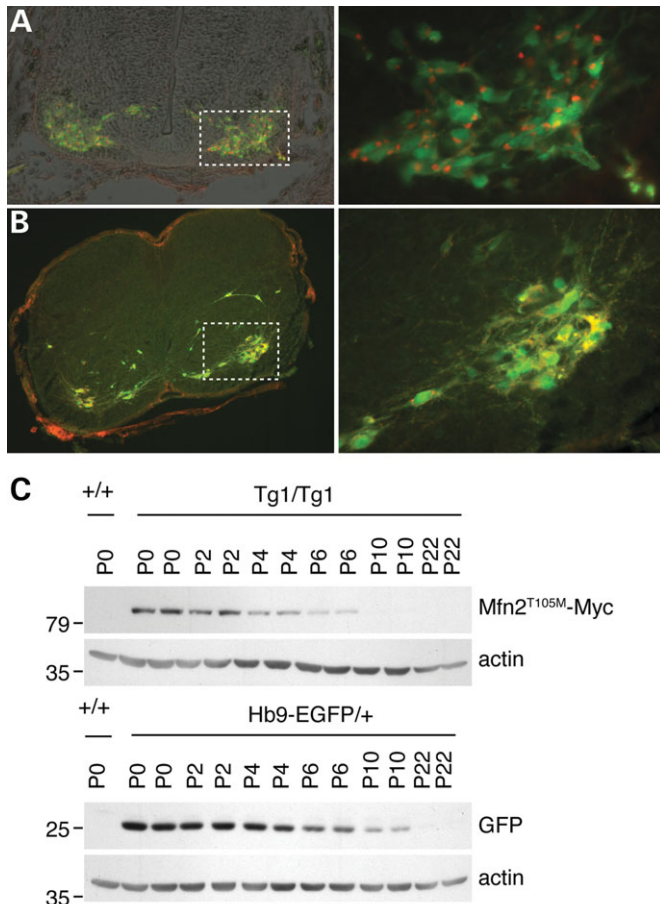


Figure 2. Transgene expression in motor neurons. (A) Cryosection of spinal column from an embryonic day 12.5 *Mfn2*^{T105M}/*Mfn2*^{T105M} embryo. GFP-labeled motor neurons (green) are located in the ventral region. Anti-Myc staining (red) detects mitochondrial localization of *Mfn2*^{T105M}-Myc within GFP-positive cells. The right panel shows details of the boxed region. (B) Immunostaining of a spinal cord cryosection from a postnatal P0 *Mfn2*^{T105M}/*Mfn2*^{T105M} animal, stained as in (A). (C) Expression time-course of HB9-*Mfn2*^{T105M} (top panels) and HB9-EGFP (bottom panels). Two spinal cord lysates were prepared from *Mfn2*^{T105M}/*Mfn2*^{T105M} and HB9-EGFP animals at the indicated ages and analyzed by western blotting using anti-Myc and anti-GFP antibodies. A β -actin antibody was used to control for protein loading.

Mfn2^{T105M} animals are clearly smaller in size (data not shown). However, because these muscles are small and difficult to dissect, we were unable to quantify the differences.

Loss of motor axons in homozygous *Mfn2*^{T105M} animals

The hindlimb defects in homozygous *Mfn2*^{T105M} animals are suggestive of a motor neuropathy. Motor neuron cell bodies reside in the ventral horns of the spinal cord, and each motor neuron sends a single axon down the spinal column. Bundles of axons, termed roots, exit the spinal column at junctions between the vertebrae. Each root has a characteristic number of axons. Because motor roots of the lumbar spine innervate the hind limbs, we quantified motor axons in the L4 and L5 nerve roots.

Our analysis indicates that motor roots in homozygous transgenic animals have fewer motor axons. Upon dissection, the lumbar motor roots appear grossly smaller in *Mfn2*^{T105M}/*Mfn2*^{T105M} animals compared with wild-type and *Mfn2*^{T105M}/+ littermates. Quantitative analysis of thin plastic sections revealed that *Mfn2*^{T105M}/*Mfn2*^{T105M} motor roots at L4 and L5 contain ~40% fewer axons compared with controls (Fig. 5A and B). In addition, we found that this loss of motor axons is most severe in the small caliber class of axons (Fig. 5C). Consistent with the motor-specific expression of the HB9-driven transgene, we did not find a significant reduction in the number of axons in sensory roots of homozygous transgenic animals (data not shown).

Mitochondrial abnormalities in homozygous *Mfn2*^{T105M} motor neurons

Given that the *Mfn2*^{T105M} allele can cause defects in mitochondrial distribution (13,14), we examined the morphology and distribution of mitochondria in transgenic motor neurons. As a wild-type control, we examined mitochondria in motor neurons cultured from HB9-EGFP embryos. In wild-type motor neurons, abundant mitochondrial tubules are distributed throughout long axonal projections (Fig. 6A). In contrast, many homozygous *Mfn2*^{T105M} motor neurons have highly aggregated mitochondria that cluster along the axon with uneven distribution (Fig. 6A). Quantitation of these results confirmed that homozygous *Mfn2*^{T105M} neurons have a severe mitochondrial distribution defect, with heterozygous *Mfn2*^{T105M} neurons having an intermediate phenotype (Fig. 6B).

DISCUSSION

By expressing the pathogenic CMT2A allele *Mfn2*^{T105M} in mouse motor neurons, we have generated a mouse line that recapitulates some of the motor defects observed in CMT2A patients. Transgenic mice show a striking inability to dorsiflex their hindpaws, resulting in an abnormal gait with foot dragging. This distal limb weakness resembles that found in CMT2A patients, who often exhibit foot-drop and a compensatory high gait. Also like CMT2A patients, the transgenic mice develop deformities in the foot. The gait defects in the transgenic mice arise from reduced numbers of motor axons, similar to the axonopathy of long peripheral nerves found in CMT2A patients. Interestingly, the axonopathy found in our transgenic model does not result in obvious loss of motor neuron cell bodies. We quantified motor neurons cell bodies along the lumbar region by Cresyl violet staining and found no significant decrease (data not shown). Even though transgene expression levels are reduced shortly after birth, the phenotype does not improve with age, likely because the affected motor neurons are too severely affected.

The peripheral neuropathy found in these animals is associated with greatly reduced mass in the anterior calf muscles. This defect of the anterior calf muscles is likely secondary to the motor axonopathy, because expression of the transgene in the calf is limited to the peripheral nerves and is not found in the muscle fibers (data not shown). Because the HB9-driven transgene is expressed embryonically, and the anterior leg

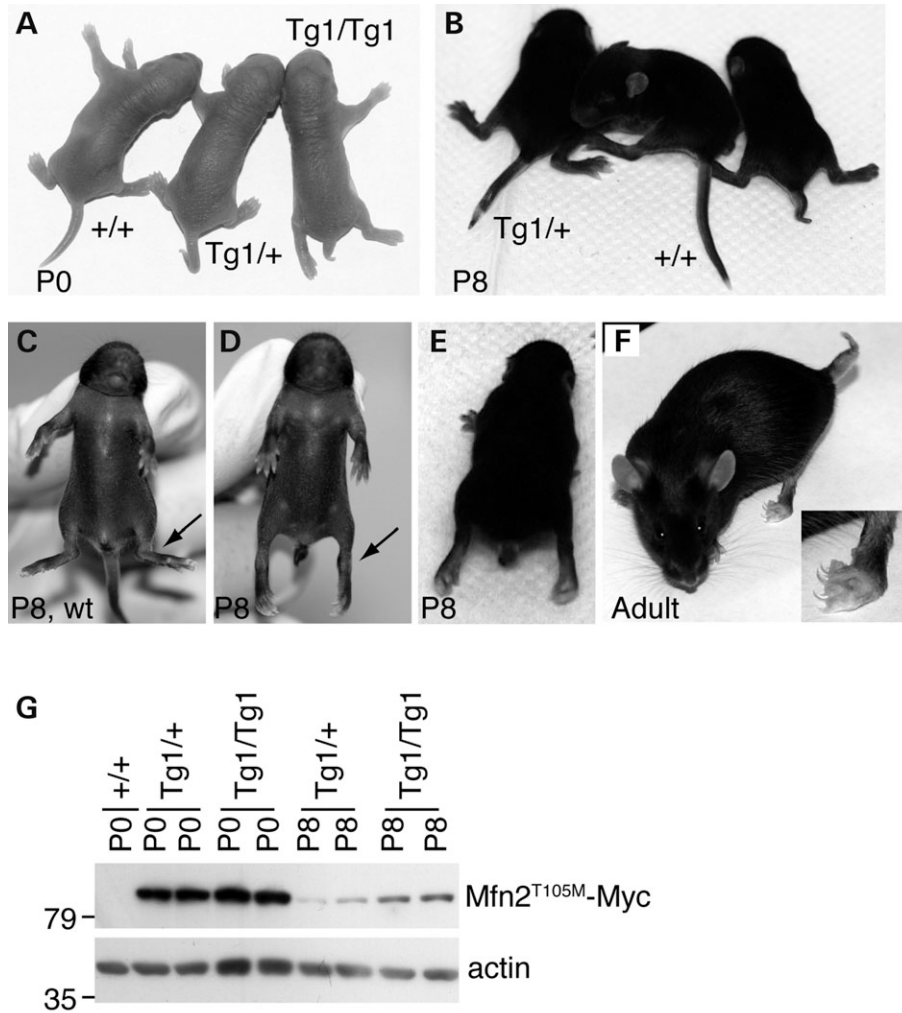


Figure 3. Limb and tail defects in *Mfn2*^{T105M} mice. (A and B) Tail defects in newborn P0 (A) and P8 (B) mice. The genotypes of the animals are indicated. Heterozygous animals have a kinked, slightly shortened tail, whereas homozygous animals have a severely shortened tail. (C and D) Hindpaw posture in P8 wild-type (C) and homozygous (D) animals. Note that the homozygous animal has limp hindpaws and is unable to dorsi-flex at the ankle (arrow). (E) Frame from a video of a P8 homozygous animal while walking. The hindpaws are extended behind, and the animal walks by pushing against the hind-knuckles. (F) Clenched and deformed hindpaw in an adult homozygous animal, detailed in inset. (G) Comparison of transgene expression levels between heterozygous and homozygous transgenic animals. Spinal cord lysates from the indicated animals were analyzed by western blotting with an anti-Myc antibody.

muscles are deficient at birth, it is possible that the defect results from a failure of muscle development rather than muscle atrophy due to loss of innervation. At present, we do not understand why the anterior leg muscles are preferentially affected, but intriguingly, the anterior leg muscles also appear to be more severely affected in CMT patients. It is possible that a subset of motor neurons is more susceptible to altered mitochondrial dynamics.

We have previously shown that most CMT2A mutations, including T105M, result in loss of Mfn2 fusion activity (13). Such non-functional Mfn2 alleles can be functionally complemented by wild-type Mfn1 but not Mfn2, and we proposed a model to explain how the autosomal dominant inheritance pattern of CMT2A may be caused by vulnerability in cells that have low Mfn1 activity (13). In contrast, our current results suggest that dominant effects of *Mfn2* disease alleles may also contribute to the autosomal dominant inheritance

pattern of CMT2A. In this transgenic model, the motor neuron defects are associated with improper distribution of mitochondria within axonal processes. This improper distribution of mitochondria is due to the ability of the *Mfn2*^{T105M} transgene to dominantly promote mitochondrial aggregation (Fig. 6) (13,14), resulting in sequestration of mitochondria to small clusters in the axons in many motor neurons. It is likely that improper mitochondrial recruitment to axons results in the observed axonopathy. Taken together, our results suggest that *Mfn2* disease alleles may affect mitochondrial dynamics by at least two distinct mechanisms.

It should be noted that *Mfn2* disease alleles disrupt mitochondrial distribution only when over-expressed (13,14). We have constructed knock-in mice containing *Mfn2* disease alleles expressed from the endogenous *Mfn2* locus. Cells from such animals do not show obvious mitochondrial distribution defects (13), and heterozygous mice do not show

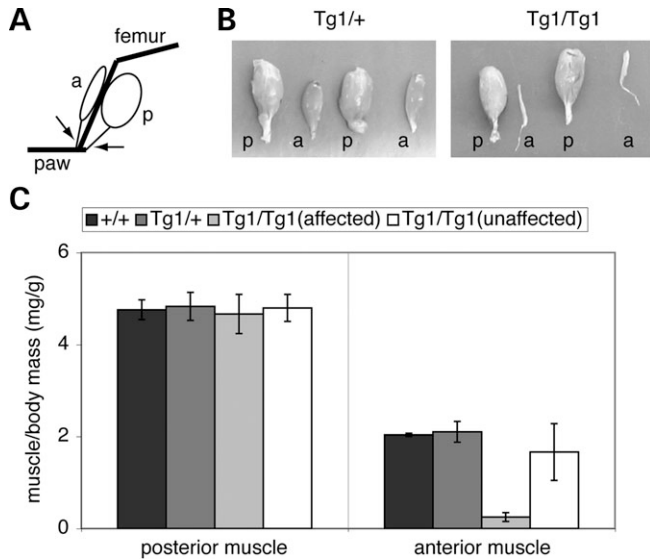


Figure 4. Reduced hindlimb muscle mass in homozygous transgenic animals. (A) Schematic of hindlimb muscle dissection. Anterior (a) and posterior (p) muscle groups were identified by the distal tendon insertion sites, as indicated by the arrows. (B) Images of dissected muscles from heterozygous and homozygous (bilaterally affected) animals at P22. Posterior muscles (p) are comparable in size in animals of both genotypes, whereas anterior muscles (a) are much smaller in homozygous animals. (C) Quantitation of posterior and anterior muscle masses from +/+ ($n=2$), $Mfn2^{T105M}/+$ ($n=18$), $Mfn2^{T105M}/Mfn2^{T105M}$ affected ($n=14$) and $Mfn2^{T105}/Mfn2^{T105M}$ unaffected ($n=8$) hind limbs. The error bars indicate standard deviations.

neuropathy. It seems likely that the much longer peripheral nerves of humans (compared with mouse) are substantially more sensitive to subtle perturbations in mitochondrial fusion. For this reason, our mouse model of CMT2A requires over-expression of $Mfn2^{T105M}$ to exaggerate its dominant effects. In the only ultrastructural study of mitochondria in the peripheral nerves of CMT2A patients, aggregation of mitochondria was a prominent feature (11). In future studies, it will be important to address more definitively the mitochondrial defects found in the peripheral nerves of CMT2A patients. Intriguingly, loss of $Mfn2$ can also lead to mitochondrial distribution defects. In mice lacking $Mfn2$, mitochondria fail to distribute properly in the dendritic extensions of Purkinje cells in the cerebellum, leading to loss of dendritic growth and cell degeneration (24). Therefore, it appears that mitochondrial distribution in neurons is highly sensitive to precise control of mitochondrial fusion and can be disrupted by both gain-of-function and loss-of-function alleles of $Mfn2$.

Our transgenic mouse line provides evidence for the importance of proper mitochondrial dynamics in motor axons. The $Mfn2^{T105M}$ allele disrupts the distribution of mitochondria to axons and results in axonopathy. Our results support growing evidence that mitochondria are vital to the function of neuronal processes. Mitochondrial recruitment to pre- and post-synaptic sites in cultured hippocampal and cortical neurons is regulated by synaptic activity and is important for growth of dendritic spines and synapses (25,26). In *Drosophila*, mitochondria must be recruited to axon terminals to provide ATP for energy-dependent processes and to maintain calcium homeostasis during prolonged nerve stimulation (16–18). Mitochondrial recruitment would be expected to be

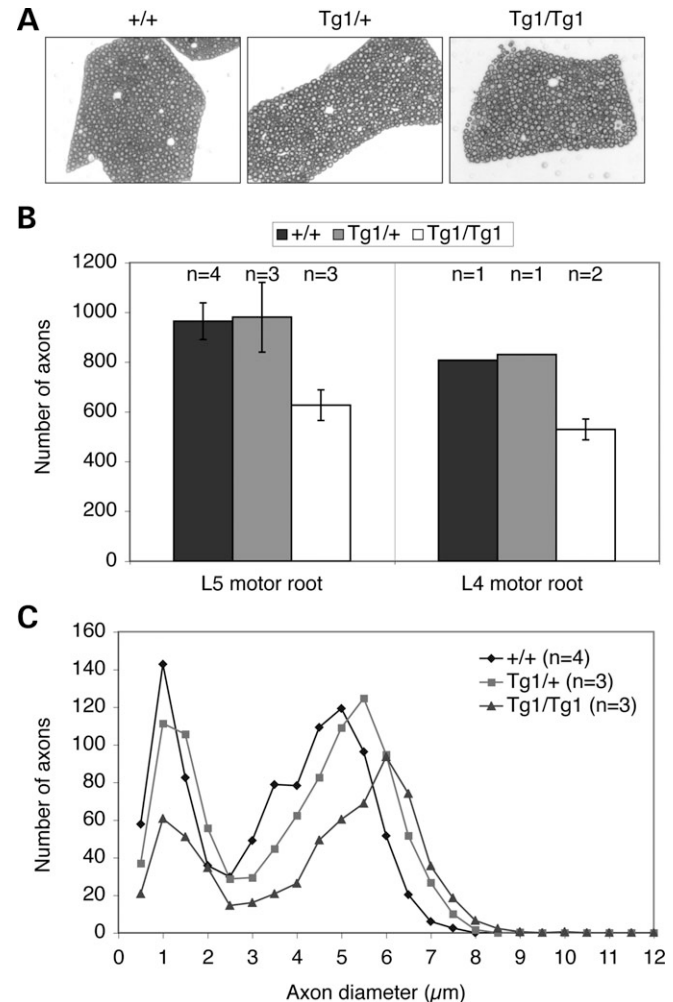


Figure 5. Reduced axon numbers in transgenic motor roots. (A) Plastic sections of L5 motor roots from 6-week-old animals stained with Toluidine blue. Genotypes are indicated. (B) Axon quantitation in L5 and L4 motor roots. The number (n) of roots counted for each genotype is indicated, and error bars indicate the standard error of the mean (SEM). The P -value is 0.002 between homozygous and wild-type samples. (C) Distribution of motor neuron axon caliber in L5 roots. Axons diameters were measured and placed into bins with 0.5 μm increments (e.g. 0–0.5, 0.5–1, 1–1.5 μm).

important for mammalian motor neurons, which have densely packed mitochondria at the nerve terminals (15). Our transgenic line provides a model system to examine this issue and to gain insights into the pathogenesis of CMT2A.

MATERIALS AND METHODS

Generation of transgenic mice

To construct the transgene, a PmeI/XhoI fragment containing C-terminally tagged $Mfn2^{T105M}$ -Myc (13) was blunted with Kenow enzyme and inserted into the PmeI site of HB9-MCS-IRES-GFP (gift of Tom Jessell, Columbia University) to generate HB9- $Mfn2^{T105M}$ -Myc-IRES-EGFP. For pronuclear injections, the plasmid was linearized by XhoI digestion, gel-purified and filter-sterilized. The linearized DNA was injected

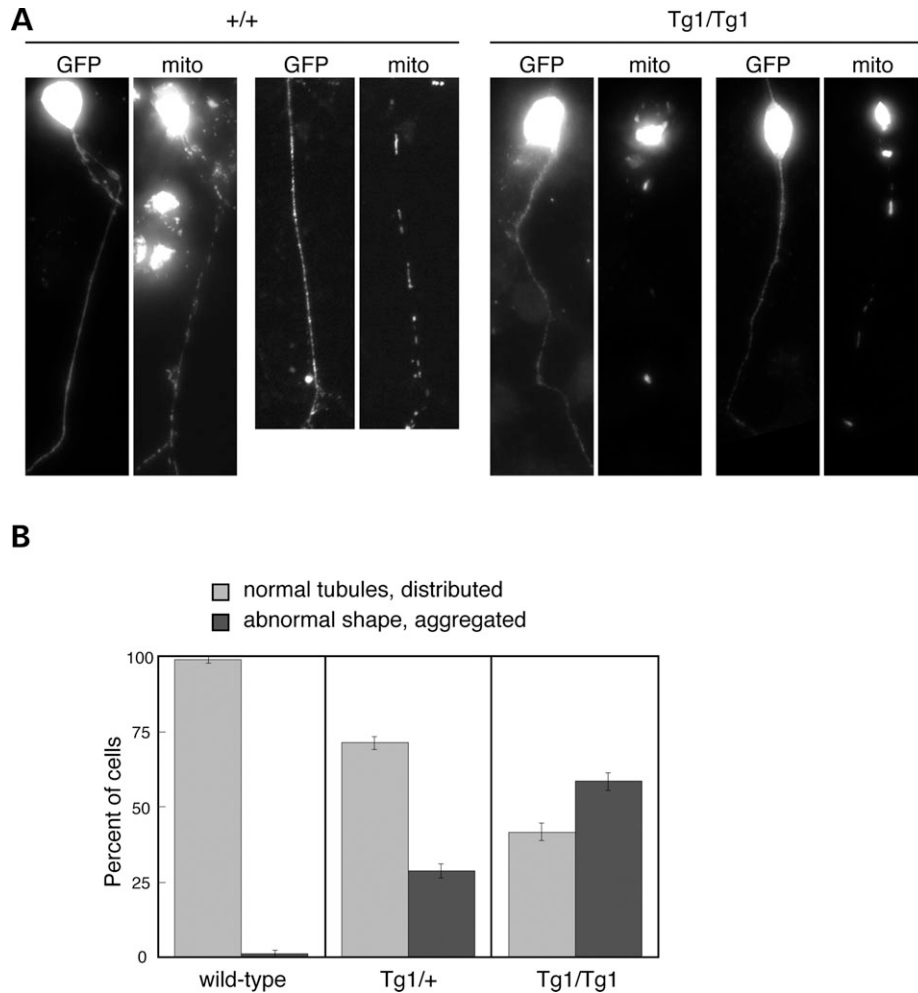


Figure 6. Altered mitochondrial distribution in *Mfn2*^{T105}/*Mfn2*^{T105M} motor neurons. (A) Images of cultured motor neurons and mitochondrial localization. Spinal cord cultures were grown from embryonic day 12.5 embryos, and motor neurons were identified by EGFP expression. Mitochondrial morphology in wild-type HB9-EGFP motor neurons (left panels) was evaluated by expression of mitochondrially targeted DsRed. Mitochondria in *Mfn2*^{T105}/*Mfn2*^{T105M} motor neurons (right panels) were evaluated by anti-Myc immunofluorescence, which identifies mitochondrially localized *Mfn2*^{T105M}-Myc. Note that in the transgenic motor neurons, the mitochondria fail to distribute evenly along the axon. *Mfn2*^{T105}/*Mfn2*^{T105M} motor neurons have aggregated mitochondria in the cell soma, but this aggregation is obscured in the images because overexposure was necessary to visualize the axonal mitochondria. (B) Quantitation of mitochondrial morphology and distribution. Normal motor neurons have thin tubular mitochondria that are distributed along the length of the axon. GFP-positive motor neurons were scored as having abnormal shape and aggregated when mitochondria were found to have non-tubular shapes and in tight clusters in the axon. Errors bars represent SEM from three trials. Both heterozygous (*P*-value, 0.0004) and homozygous cultures (*P*-value, 0.0001) had significantly higher levels of abnormal motor neurons. In addition, the differences between homozygous and heterozygous cultures were also significant (*P*-value, 0.0013).

at the Caltech Transgenic and Knockout Core Facility. Injected embryos were implanted into pseudo-pregnant females. Founder animals were screened using the PCR assay depicted in Figure 1, where primer A is 5'-GCGCCTCTCTGTGCTAGTTG and primer B is 5'-GTCTGCAGTGAACCTGGCAAT.

The transgene insertion site in the *Mfn2*^{T105M} line was cloned using an inverse PCR strategy (27). *Mfn2*^{T105M} genomic DNA was digested with *EcoRI* (present in the 3' end of the transgene), self-ligated and used as a template for PCR with divergent GFP primers. The PCR product was cloned and identified by sequencing. This integration site was confirmed with the PCR assay depicted in Figure 1. The primers used were: C (5'-TGGGGTGTGCTTTATTGACA), D (5'-CTGCTTTCATGCACACACCT), E (5'-CTGCTTTCATGCACACACCT) and F (5'-GCCTTCTTGAGAACCTGTGC).

Cryosection and immunofluorescence

For immunostaining, embryonic day 12.5 embryos were fixed in 4% paraformaldehyde in phosphate buffered saline (PBS) for 2 h at 4°C, washed in PBS, equilibrated with 30% sucrose in PBS and frozen in Tissue-Tek O.C.T. compound. Embryos were sectioned with a Microm HM550 cryostat at -20°C, air-dried and then immunostained with the anti-Myc 9E10 monoclonal antibody and a Cy3-labeled secondary antibody. EGFP signal was enhanced with an Alexa-488 conjugated anti-GFP antibody (Invitrogen).

Spinal cord lysates

The thoracic spinal cord was extruded with PBS and immediately Dounce-homogenized in Tris-buffered saline (pH 8.0)

containing 1% Triton X-100 and a protease inhibitor cocktail (Roche). Lysates were cleared by centrifugation, and protein levels were quantified with the BioRad Protein Assay kit. Equivalent loads were analyzed by western blotting.

Hindlimb muscle analysis

P22 animals were euthanized, and skin was removed from the hindlimbs. Anterior and posterior muscles groups were identified by the insertion site of the distal tendon (Fig. 4A). The muscles were cut at the distal insertion point, lifted away from the limb and severed at the proximal attachment site. This technique allowed for reproducible isolation of the same muscle groups in different animals, despite differences in muscle size. Muscles were weighed immediately following dissection.

Motor root dissection and staining

L4 and L5 motor and sensory roots were dissected from six-week-old animals following transcardial perfusion with 4% paraformaldehyde in PBS. Dissected roots were further fixed and processed for embedment in epon plastic for thin sectioning, as described previously (28). Thin sections were stained with Toluidine blue to visualize myelin. BIOQUANT software was used to count axons and to measure individual axon diameters.

Motor neuron cultures

Spinal columns were dissected from embryonic day 12.5 embryos and dissociated using Papain protease (Worthington). The cells were plated on cover slips treated with Matrigel (BD Biosciences), and the motor neurons were cultured as described previously (20). HB9-EGFP cultures were infected with lentivirus encoding mitochondrially targeted DsRed. 48 or 72 h later, the cultures were processed for immunofluorescence. *Mfn2*^{T105M} cultures were probed with the anti-Myc antibody 9E10 and a Cy3 labeled secondary. The EGFP signal in both cultures was enhanced using an Alexa-488 conjugated anti-GFP antibody (Invitrogen).

SUPPLEMENTARY MATERIAL

Supplementary Material is available at HMG Online.

ACKNOWLEDGEMENTS

We thank Tim Miller, John Griffin and members of the Chan lab for helpful discussions; Tom Jessell for the HB9-EGFP mice and the HB9-IRES-EGFP cloning vector; Diane Solis and Gwen Williams for invaluable mouse support and Shirley Pease for directing pronuclear injections at the Caltech Transgenic and Knockout Core Facility.

FUNDING

C.V.V. is funded by a Development Grant from the Muscular Dystrophy Association. D.W.C. receives salary support from

the Ludwig Institute. This work was supported by NIH grant GM062967 to D.C.C.

Conflict of Interest statement. None declared.

REFERENCES

- Young, P. and Suter, U. (2003) The causes of Charcot–Marie–Tooth disease. *Cell. Mol. Life Sci.*, **60**, 2547–2560.
- Zuchner, S. and Vance, J.M. (2006) Mechanisms of disease: a molecular genetic update on hereditary axonal neuropathies. *Nat. Clin. Pract. Neurol.*, **2**, 45–53.
- Zuchner, S., Mersyanova, I.V., Muglia, M., Bissar-Tadmouri, N., Rochelle, J., Dadali, E.L., Zappia, M., Nelis, E., Patitucci, A., Senderek, J. *et al.* (2004) Mutations in the mitochondrial GTPase mitofusin 2 cause Charcot–Marie–Tooth neuropathy type 2A. *Nat. Genet.*, **36**, 449–451.
- Griffin, E.E., Detmer, S.A. and Chan, D.C. (2006) Molecular mechanism of mitochondrial membrane fusion. *Biochim. Biophys. Acta*, **1763**, 482–489.
- Chan, D.C. (2006) Mitochondrial fusion and fission in mammals. *Annu. Rev. Cell Dev. Biol.*, **22**, 79–99.
- Okamoto, K. and Shaw, J.M. (2005) Mitochondrial morphology and dynamics in yeast and multicellular eukaryotes. *Annu. Rev. Genet.*, **39**, 503–536.
- Chung, K.W., Kim, S.B., Park, K.D., Choi, K.G., Lee, J.H., Eun, H.W., Suh, J.S., Hwang, J.H., Kim, W.K., Seo, B.C. *et al.* (2006) Early onset severe and late-onset mild Charcot–Marie–Tooth disease with mitofusin 2 (MFN2) mutations. *Brain*, **129**, 2103–2118.
- Engelfried, K., Vorgerd, M., Hagedorn, M., Haas, G., Gilles, J., Epplen, J.T. and Meins, M. (2006) Charcot–Marie–Tooth neuropathy type 2A: novel mutations in the mitofusin 2 gene (MFN2). *BMC Med. Genet.*, **7**, 53.
- Kijima, K., Numakura, C., Izumino, H., Umetsu, K., Nezu, A., Shiiiki, T., Ogawa, M., Ishizaki, Y., Kitamura, T., Shozawa, Y. *et al.* (2005) Mitochondrial GTPase mitofusin 2 mutation in Charcot–Marie–Tooth neuropathy type 2A. *Hum. Genet.*, **116**, 23–27.
- Lawson, V.H., Graham, B.V. and Flanigan, K.M. (2005) Clinical and electrophysiologic features of CMT2A with mutations in the mitofusin 2 gene. *Neurology*, **65**, 197–204.
- Verhoeven, K., Claeys, K.G., Zuchner, S., Schroder, J.M., Weis, J., Ceuterick, C., Jordanova, A., Nelis, E., De Vriendt, E., Van Hul, M. *et al.* (2006) MFN2 mutation distribution and genotype/phenotype correlation in Charcot–Marie–Tooth type 2. *Brain*, **129**, 2093–2102.
- Zuchner, S., De Jonghe, P., Jordanova, A., Claeys, K.G., Guergueltcheva, V., Cherninkova, S., Hamilton, S.R., Van Stavern, G., Krajewski, K.M., Stajich, J. *et al.* (2006) Axonal neuropathy with optic atrophy is caused by mutations in mitofusin 2. *Ann. Neurol.*, **59**, 276–281.
- Detmer, S.A. and Chan, D.C. (2007) Complementation between mouse Mfn1 and Mfn2 protects mitochondrial fusion defects caused by CMT2A disease mutations. *J. Cell Biol.*, **176**, 405–414.
- Baloh, R.H., Schmidt, R.E., Pestronk, A. and Milbrandt, J. (2007) Altered axonal mitochondrial transport in the pathogenesis of Charcot–Marie–Tooth disease from mitofusin 2 mutations. *J. Neurosci.*, **27**, 422–430.
- Misgeld, T., Kerschensteiner, M., Bareyre, F.M., Burgess, R.W. and Lichtman, J.W. (2007) Imaging axonal transport of mitochondria in vivo. *Nat. Methods*, **4**, 559–561.
- Stowers, R.S., Megeath, L.J., Gorska-Andrzejak, J., Meinertzhagen, I.A. and Schwarz, T.L. (2002) Axonal transport of mitochondria to synapses depends on Milton, a novel Drosophila protein. *Neuron*, **36**, 1063–1077.
- Guo, X., Macleod, G.T., Wellington, A., Hu, F., Panchumarthi, S., Schoenfield, M., Marin, L., Charlton, M.P., Atwood, H.L. and Zinsmaier, K.E. (2005) The GTPase dMiro is required for axonal transport of mitochondria to Drosophila synapses. *Neuron*, **47**, 379–393.
- Verstreken, P., Ly, C.V., Venken, K.J., Koh, T.W., Zhou, Y. and Bellen, H.J. (2005) Synaptic mitochondria are critical for mobilization of reserve pool vesicles at Drosophila neuromuscular junctions. *Neuron*, **47**, 365–378.
- Bourne, H.R., Sanders, D.A. and McCormick, F. (1991) The GTPase superfamily: conserved structure and molecular mechanism. *Nature*, **349**, 117–127.
- Wichterle, H., Lieberam, I., Porter, J.A. and Jessell, T.M. (2002) Directed differentiation of embryonic stem cells into motor neurons. *Cell*, **110**, 385–397.

21. Arber, S., Han, B., Mendelsohn, M., Smith, M., Jessell, T.M. and Sockanathan, S. (1999) Requirement for the homeobox gene Hb9 in the consolidation of motor neuron identity. *Neuron*, **23**, 659–674.
22. Thaler, J., Harrison, K., Sharma, K., Lettieri, K., Kehrl, J. and Pfaff, S.L. (1999) Active suppression of interneuron programs within developing motor neurons revealed by analysis of homeodomain factor HB9. *Neuron*, **23**, 675–687.
23. Hsieh-Li, H.M., Chang, J.G., Jong, Y.J., Wu, M.H., Wang, N.M., Tsai, C.H. and Li, H. (2000) A mouse model for spinal muscular atrophy. *Nat Genet*, **24**, 66–70.
24. Chen, H., McCaffery, J.M. and Chan, D.C. (2007) Mitochondrial fusion protects against neurodegeneration in the cerebellum. *Cell*, **130**, 548–562.
25. Chang, D.T., Honick, A.S. and Reynolds, I.J. (2006) Mitochondrial trafficking to synapses in cultured primary cortical neurons. *J. Neurosci.*, **26**, 7035–7045.
26. Li, Z., Okamoto, K., Hayashi, Y. and Sheng, M. (2004) The importance of dendritic mitochondria in the morphogenesis and plasticity of spines and synapses. *Cell*, **119**, 873–887.
27. Li, J., Shen, H., Himmel, K.L., Dupuy, A.J., Largaespada, D.A., Nakamura, T., Shaughnessy, J.D., Jr, Jenkins, N.A. and Copeland, N.G. (1999) Leukaemia disease genes: large-scale cloning and pathway predictions. *Nat. Genet.*, **23**, 348–353.
28. Yamanaka, K., Miller, T.M., McAlonis-Downes, M., Chun, S.J. and Cleveland, D.W. (2006) Progressive spinal axonal degeneration and slowness in ALS2-deficient mice. *Ann. Neurol.*, **60**, 95–104.